CHEMISTRY OF MATERIALS
Article

Chem. Mater. **2009,** *21,* 3629–3637 3629
DOI:10.1021/cm900874u

Macroporous Silica Hollow Microspheres as Nanoparticle Collectors

Ling Li, Jun Ding, and Junmin Xue*

Department of Materials Science and Engineering, National University of Singapore, Singapore 117576, Republic of Singapore

Received March 30, 2009. Revised Manuscript Received July 1, 2009

In this work, we report the fabrication of macroporous silica hollow microspheres through a polystyrene (PS) templating route. Silica seeds are first deposited onto the surfaces of PS beads as a result of the hydrolysis and condensation of tetraethyl orthosilicate (TEOS) in a basic condition. Subsequent growth of silica seeds to nanoparticles with size of ~40 nm leads to the coalescence of the adjacent particles, forming continuous two-dimensional silica networks on the PS surfaces. The uncovered areas on PS surfaces were converted into macrosized through holes after core removal through either dissolution or calcination, thus forming the macroporous silica hollow structures. The monodispersed hollow spheres were demonstrated to be efficient collectors for capturing and loading various nanoparticles, both hydrophilic and hydrophobic, from the external solutions. The functional particles loaded macroporous hollow spheres will have promising applications in biotechnology and catalysis.

Introduction

The fabrication of well-defined structures in the submicrometer range has attracted increasing research interest in recent years. Synthesis of nano/microsized hollow spheres with empty interior, in particular, has been one of the most active research areas because of their technical importance in a variety of applications, including nanoreactors, drug delivery carriers, building blocks for photonic crystals, catalyst carriers, and nanocapsules for hydrogen storage.[1−13] Most fabrication approaches rely on the template-assisted synthesis, and the templates employed include various nano/microparticles,[12,14−16] emulsions,[17,18] and vesicles,[19,20] although there has been an increase in the number of reports on novel template-free or self-templating routes for the preparation of hollow spheres.[21,22] The design of hollow microspheres with complex, specific, controllable shell structure is currently of considerable scientific and technological interests.[23,24] For example, hollow spheres with mesoporous shells have received much attention because of the importance in various promising applications, especially in drug delivery systems. [25,26] However, access of large entities, such as proteins and DNA, through these shells with pores < 10 nm is often a slow process or even impossible.

To combat this challenge, several research groups have investigated the synthesis of hollow structures with microthrough-holes on the shells. For example, hollow

*To whom all correspondence should be addressed. Phone: 65 6516 4655. Fax: 65 6776 3604. E-mail: msexuejm@nus.edu.sg.

(1) Caruso, F.; Caruso, A.; Mohwald, H. *Science* **1998**, *282*, 1111–1114.
(2) Lou, X. W.; Yuan, C.; Rhoades, E.; Zhang, Q.; Archer, L. A. *Adv. Funct. Mater.* **2006**, *16*, 1679–1684.
(3) Shchukin, D. G.; Sukhorukov, G. B. *Adv. Mater.* **2004**, *16*, 671–682.
(4) Choi, W. S.; Park, J. H.; Yoo, H. Y.; Kim, J. Y.; Cho, B. K.; Kim, D. Y. *Angew. Chem., Int. Ed.* **2005**, *44*, 1096–1101.
(5) Hah, H. J.; Um, J. I.; Han, S. H.; Koo, S. M. *Chem. Commun.* **2004**, 1012–1013.
(6) Yang, J.; Lee, J.; Kang, J.; Lee, K.; Suh, J.-S.; Yoon, H.-G.; Huh, Y.-M.; Haam, S. *Langmuir* **2008**, *24*, 3417–3421.
(7) Zhu, Y. F.; Shi, J. L.; Shen, W. H.; Dong, X. P.; Feng, J. W.; Ruan, M. L.; Li, Y. Si *Angew. Chem., Int. Ed.* **2005**, *44*, 5083–5087.
(8) Lu, Y.; McLellan, J.; Xia, Y. *Langmuir* **2004**, *20*, 3464–3470.
(9) Ikeda, S.; Ishino, S.; Harada, T.; Okamoto, N.; Sakata, T.; Mori, H.; Kuwabata, S.; Torimoto, T.; Matsumura, M. *Angew. Chem., Int. Ed.* **2006**, *45*, 7063–7066.
(10) Liang, H. P.; Zhang, H. M.; Hu, J. S.; Guo, Y. G.; Wang, L. J.; Bai, C. L. *Angew. Chem., Int. Ed.* **2004**, *43*, 1540–1543.
(11) Lee, K. T.; Jung, Y. S.; Oh, S. M. *J. Am. Chem. Soc.* **2003**, *125*, 5652–5623.
(12) Kim, S.-W.; Kim, M.; Lee, W. Y.; Hyeon, T. *J. Am. Chem. Soc.* **2002**, *124*, 7642–7643.
(13) Miyao, T.; Minoshima, K.; Naito, S. *J. Mater. Chem.* **2005**, *15*, 2268–2270.
(14) Chen, M.; Wu, L.; Zhou, S.; You, B. *Adv. Mater.* **2006**, *18*, 801–806.
(15) Zou, H.; Wu, S.; Ran, Q.; Shen, J. *J. Phys. Chem. C* **2008**, *112*, 11623–11629.
(16) Yang, Z. Z.; Niu, Z. W.; Lu, Y. F.; Hu, Z. B.; Han, C. C. *Angew. Chem., Int. Ed.* **2003**, *42*, 1943–1945.
(17) Schacht, S.; Huo, Q.; Voigt-Martin, I. G.; Stucky, C. D.; Schuth, F. *Science* **1996**, *273*, 768–771.
(18) Botterhuis, N. E.; Sun, Q.; Magusin, P. C. M. M.; van Santen, R. A.; Sommerdijk, N. A. J. M. *Chem.—Eur. J.* **2006**, *12*, 1448–1456.
(19) Djojoputro, H.; Zhou, X. F.; Qiao, S. Z.; Wang, L. Z.; Yu, C. Z.; Lu, G. Q. *J. Am. Chem. Soc.* **2006**, *128*, 6320–6321.
(20) Yeh, Y. Q.; Chen, B. C.; Lin, H. P.; Tang, C. Y. *Langmuir* **2006**, *22*, 6–9.
(21) Yin, Y. D.; Rioux, R. M.; Erdonmez, C. K.; Hughes, S.; Somorjai, G. A.; Alivisatos, A. P. *Science* **2004**, *304*, 711–714.
(22) Zhang, T.; Ge, J.; Hu, Y.; Zhang, Q.; Aloni, S.; Yin, Y. *Angew. Chem., Int. Ed.* **2008**, *47*, 5806–5811.
(23) Wang, J.; Xiao, Q.; Zhou, H.; Sun, P.; Yuan, Z.; Li, B.; Ding, D.; Shi, A.-C.; Chen, T. *Adv. Mater.* **2006**, *18*, 3284–3288.
(24) Yu, M.; Wang, H.; Zhou, X.; Yuan, P.; Yu, C. *J. Am. Chem. Soc.* **2007**, *129*, 14576–14577.
(25) Zhang, L.; Qiao, S. Z.; Jin, Y. G.; Chen, Z. G.; Gu, H. C.; Lu, G. Q. *Adv. Mater.* **2008**, 805–809.
(26) Zhao, W.; Chen, H.; Li, Y.; Li, L.; Lang, M.; J., Shi *Adv. Funct. Mater.* **2008**, 2780–2788.

Published on Web 07/20/2009

polystyrene capsules with single open hole have been fabricated through a swelling and fast cooling process.[27,28] Functional nanoparticles were also successfully encapsulated through the holes, which could be further closed up by thermal annealing or solvent treatment. Han et al. obtained poly(o-methoxyaniline) hollow microspheres with similar structure through a chemical polymerization route, where the diffusion of monomers during this process was responsible for the formation of the hole.[29] Yoshizawa et al. demonstrated a unique phase-separation method for preparing microcapsules (size ~10 μm) with holes in their shells.[30] In this approach, the hole size could be precisely controlled by adjusting two types of surfactants, i.e., water-soluble surfactant molecules for shell formation and oil-soluble surfactant molecules for hole formation. Though lagging behind, silica hollow spheres with macroporous shell have been successfully fabricated in several reports. Compared with polymer, silica has been demonstrated to be nontoxic, and more stable.[31−33] By adding certain water-soluble polymers to a solution of water/oil/water double emulsion system, Fujiwara et al. synthesized silica hollow spheres with nano/macro-holes like diatomaceous earth structure.[34] Shiomi et al. obtained similar structure by calcination of lysozyme−silica hybrid particles, and the ship-in-bottle encapsulation of proteins into the porous structure was realized.[35,36] However, all these reported methods require either stringent control of emulsion system or high-temperature treatment (up to 700 °C), which makes the synthesis process tedious and difficult to control. Moreover, silica hollow microspheres obtained through these methods are often not uniform in size, which might jeopardize the practical applications and quantitative analysis. Therefore, facile and simple routes to obtain monodisperse silica hollow microspheres with macroholes in their shells are highly desirable.

Very recently, we reported a novel oil-in-diethylene glycol microemulsion route, through which silica composite nanospheres incorporated with an ultrahigh loading of superparamagnetic iron oxide nanoparticles (SPIONs) could be obtained.[37] By purposely increasing the amount of toluene in the oil phase, macroporous hollow microspheres with SPIONs loaded in their shells could be also synthesized.[38] The increase in interior pressure due to droplet contraction during the transformation of liquid tetraethyl orthosilicate (TEOS) to solid silica was believed to be the major reason for the formation of such a structure. Lim et al. also obtained nanoparticle-loaded capsules with single open hole in their shells through a similar approach but using different solvent and surfactant.[39] In this work, we demonstrated another simple, fast, and general route to synthesize monodisperse macroporous silica hollow microspheres (denoted as MSHMs) of which the through-holes in shells are >50 nm in diameter, by using polystyrene (PS) beads as template. Silica seeds are first formed at the polyvinylpyrrolidone (PVP)-modified surface of PS beads as a result of the hydrolysis and condensation of TEOS in a basic condition. Subsequent growth of silica seeds to nanoparticles with size of ~40 nm leads to the coalescence of adjacent particles, forming an intact shell consisting of connected silica nanoparticles. The uncovered areas on PS surfaces become macrosized through holes after core removal through either dissolution or calcination, thus forming MSHMs. More importantly, we demonstrate that the as-synthesized MSHMs could be used as efficient collectors for capturing and loading various nanoparticles, both hydrophilic and hydrophobic, from the external solutions.

Materials and Methods

Materials. Polyvinylpyrrolidone (PVP, MW = 55 000), 4, 4-Azobis(4-cyano-valeic acid) (ABCVA, 75%), hexadecanediol (90%), gold(III) chloride hydrate (99.9%), and Lumidot CdSe/ZnS quantum dots stabilized with a mixture of hexadecylamine and trioctylphosphine ligands (5 mg/mL) were purchased from Aldrich. Styrene (99.5%), iron(III) acetylacetonate ($Fe(acac)_3$, 97.9%), oleic acid, oleylamine (70%), and tetraethyl orthosilicate (TEOS, 99.0%) were obtained from Fluka. Sodium borohydride (98.5%), toluene (99.5%), and sodium citrate were purchased from Sigma-Aldrich. Ammonia aqueous solution (28 wt %) was obtained from Univar. All chemicals were used as received without any further purification. Absolute ethanol (analytical reagent grade) from Fisher Scientific and ultrapure water ($\approx 17\ M\Omega cm^{-1}$) from a Milli-Q water system was used throughout the experiment.

Synthesis of PVP-Modified Polystyrene (PS) Beads. The monodisperse PVP-modified PS beads were prepared through a dispersion polymerization described as follows: PVP (1.5 g), ABCVA (0.2 g), H_2O (5 g), styrene (5 g), and ethanol (22.5 g) were charged to a three-necked flask with magnetic stirring. The reaction solution was deoxygenated by bubbling nitrogen gas at room temperature for 30 min, ad was then heated to 70 °C for 1.5 h. Another 5 g of styrene and 22.5 g of ethanol were added to the system. The reaction was allowed for 6 h, and the as-prepared PS beads were collected through centrifugation and washed with absolute ethanol for 3 times. The final products were dispersed in ethanol with volume ratio to the original reaction solution of 4, which was used as stock solution for later silica encapsulations.

Synthesis of Silica MSHMs. Ten milliliters of PS stock solution in ethanol was added to a mixture containing 30 mL of ethanol, 3 mL of H_2O and 1 mL of TEOS. The mixture was

(27) Im, S. H.; Jeong, U.; Xia, Y. *Nat. Mater.* **2005**, *4*, 671–674.
(28) Jeong, U.; Im, S. H.; Camargo, P. H. C.; Kim, J. H.; Xia, Y. *Langmuir* **2007**, *23*, 10968–10975.
(29) Han, J.; Song, G.; Guo, R. *Chem. Mater.* **2007**, *19*, 973–975.
(30) Kamio, E.; Yonemura, S.; Ono, T.; Yoshizawa, H. *Langmuir* **2008**, *24*, 13287–13298.
(31) Lu, Y.; Yin, Y.; Mayers, B. T.; Xia, Y. *Nano Lett.* **2002**, *2*, 183–186.
(32) Schroedter, A.; Weller, H. *Nano Lett.* **2002**, *2*, 1363–1367.
(33) Gorelikov, I.; Matsuura, N. *Nano Lett.* **2008**, *8*, 369–373.
(34) Fujiwara, M.; Shiokawa, K.; Sakakura, I.; Nakahara, Y. *Nano Lett.* **2006**, *6*, 2925–2928.
(35) Shiomi, T.; Tsunoda, T.; Kawai, A.; Mizukami, F.; Sakaguchi, K. *Chem. Commun.* **2007**, 4404–4406.
(36) Shiomi, T.; Tsunoda, T.; Kawai, A.; Matsuura, S.-I.; Mizukami, F.; Sakaguchi, K. *Small* **2009**, *5*, 67–71.
(37) Li, L.; Choo, E. S. G.; Yi, J.; Ding, J.; Tang, X.; Xue, J. *Chem. Mater.* **2008**, *20*, 6292–6294.
(38) Li, L.; Choo, E. S. G.; Tang, X.; Ding, J.; Xue, J. *Chem. Commun.* **2008**, 938–940.
(39) Lim, Y. T.; Kim, J. K.; Noh, Y.-W.; Cho, M. Y.; Chung, B. H. *Small* **2009**, *5*, 324–328.

slowly heated up to 50 °C in an oil bath. Two and a half millilters of ammonia hydroxide was added quickly, and the reaction was terminated after 25 min. PS@SiO_2 core/shell composite beads were collected through centrifugation, washed with ethanol 3 times, and finally dispersed in absolute ethanol. The MSHMs were obtained by dissolving PS core with toluene or calcination at 450 °C for 1 h.

Synthesis of 14 nm Sized Gold Nanoparticles. Uniform gold nanoparticles, ~14 nm in diameter, were prepared by rapidly injecting a sodium citrate solution (2 mL, 40 mM) into a boiling aqueous solution of $HAuCl_4$ (20 mL, 110 ppm) under vigorous stirring. [40] After boiling for 15 min, heat was removed to cool to room temperature. The final volume was adjusted to 20 mL to compensate for the evaporation during boiling, and the as-synthesized gold colloid was used without any washing procedures.

Synthesis of Hydrophobic SPIONs. Hydrophobic SPIONs were prepared using a previously described method, which is based on the thermal decomposition of $Fe(acac)_3$. [41] Typically, 4 mmol of $Fe(acac)_3$, 20 mmol of 1,2-hexadecanediol, 12 mmol of oleic acid, 12 mmol of oleylamine, and 40 mL of benzyl ether were mixed in a round-bottom flask with nitrogen flowing under magnetic stirring. The mixture was heated to 200 °C for 2 h and then heated to reflux at 300 °C for another 2 h. The reaction solution was then cooled to room temperature and 80 mL of ethanol was added. The black product was collected by centrifugation (6000 rpm, 10 min) and dispersed in hexane with the presence of oleic acid. The SPIONs were then subjected to two cycles of precipitation in methanol and centrifugation. Finally, hydrophobic SPIONs were dispersed in toluene.

Capturing Gold Nanoparticles with MSHMs. The as-synthesized MSHMs were first dried at 50 °C for 3 h before using them to capture gold nanoparticles. Various amounts (0.8−3.2 mg) of dried MSHMs were dispersed with 2 mL of gold colloid (79.01 ppm) with magnetic stirring. The capturing process was terminated after 24 h, and the volume of solution was adjusted to 12.5 mL with H_2O. The gold nanoparticles captured by MSHMs were separated from the uncaptured ones through centrifugation at low speed (2000 rpm, 4 min) because of their much larger weight. Eleven mL of supernatant aqueous solution containing only uncaptured gold nanoparticles was carefully taken for further characterizations (denoted as SPT01−04). The remaining MSHMs loaded with gold nanoparticles were diluted with 2 mL of H_2O for UV−vis measurement (denoted as PPT01−04).

Characterizations. The morphology was examined by using field emission scanning electron microscopy (SEM; XL 30 FEG Philips, Hillsboro, OR). All transmission electron microscopy (TEM) images were obtained by using a JEOL 3010 instrument (300 kV). Samples were prepared by dipping carbon-coated copper grids into the sample solution followed by drying at room temperature. The UV−vis absorption spectra were registered by using a UV−vis−NIR spectrophotometer (Varian, Cary 5000). The concentration of gold was determined through inductively coupled plasma (ICP) analysis (PerkinElmer, Dualview Optima 5300 DV ICP-OES system, USA). Thermal gravity analysis (TGA) data were recorded by using an SDTQ600 instrument. PS beads, PS@SiO_2 beads, and MSHMs were dried at 50 °C overnight to yield dried powders before examination. The nitrogen adsorption/desorption experiments were carried out using a NOVA 3000 series instrument (Quantachrome Instruments) at −196 °C. Prior to measurements, the sample was degassed at room temperature for 6 h.

Results and Discussions

For the synthesis of MSHMs, monodisperse PS beads, which were used as templates for subsequent silica deposition, were first fabricated through a dispersion polymerization route with PVP as surfactants and stabilizers. PS beads have always been attractive spherical templates because they are relatively inexpensive and available in uniform size.[8,14] Scanning and transmission electron microscopy (SEM and TEM, respectively) observations (Figure 1A−C) demonstrated that the as-prepared PS beads had an average size of 704.6 nm, with a very narrow distribution (standard deviation smaller than 3%), as shown in the size distribution histogram (see Figure S1 in the Supporting Information). PVP-modified PS beads were directly applied as templates for silica coating without any other surface modifications. As shown in Figure 1D, after a simple sol−gel coating process for 25 min, silica nanoparticles were successfully attached onto the surface of PS beads, forming PS@SiO_2 core/shell composite beads. More importantly, it was observed that the PS surface was not fully covered with silica shells. Careful investigation revealed that the shell was actually made of connected individual primary silica nanoparticles with size of around 40 nm (**Inset,** Figure 1D). This agreed with the average diameter of PS@SiO_2 (784.4 nm), which equaled to the summation of the diameters of PS beads and silica nanoparticles (see Figure S1 in the Supporting Information). Typical PS@SiO_2 core/shell structure was observed under TEM (images E and F in Figure 1). The uneven distribution of contrast across the shell demonstrated its distinction from normal core/shell structures with uniform and smooth shells. Individual silica nanoparticles in the shell could be clearly observed in high-magnification TEM images (see Figure S2 in the Supporting Information). The amount of silica estimated from thermogravimetric analysis (TGA) was 26.4 wt % (see Figure S3 in the Supporting Information), from which the thickness of the silica shell was estimated to be 28.6 nm. This slightly smaller value compared with TEM and SEM observations is reasonable because we have assumed a fully covered uniform silica shell in calculation.

One of the most important advantages to use PS beads as template to synthesize hollow structures is that PS core can be easily removed by either calcination or solvent dissolution.[8,42] Here, we demonstrated that both approaches could be applied to obtain silica hollow structures. As shown in a typical SEM image (Figure 1G), silica hollow microspheres could be easily obtained by dissolving the PS core in toluene. The average sphere size was measured to be 794.6 nm, which is slightly bigger than that of the PS@SiO2 composite spheres (see Figure S1 in

(40) Grabar, K. C.; Freeman, R. G.; Hommer, M. B.; Natan, M. J. *Anal. Chem.* **1995**, *67*, 735–743.
(41) Sun, S.; Zeng, H.; Robinson, D. B.; Raoux, S.; Rice, P. M.; Wang, S. X.; Li, G. *J. Am. Chem. Soc.* **2004**, *126*, 273–279.
(42) Yang, J.; Lind, J. U.; Trogler, W. *Chem. Mater.* **2008**, *20*, 2875–2877.

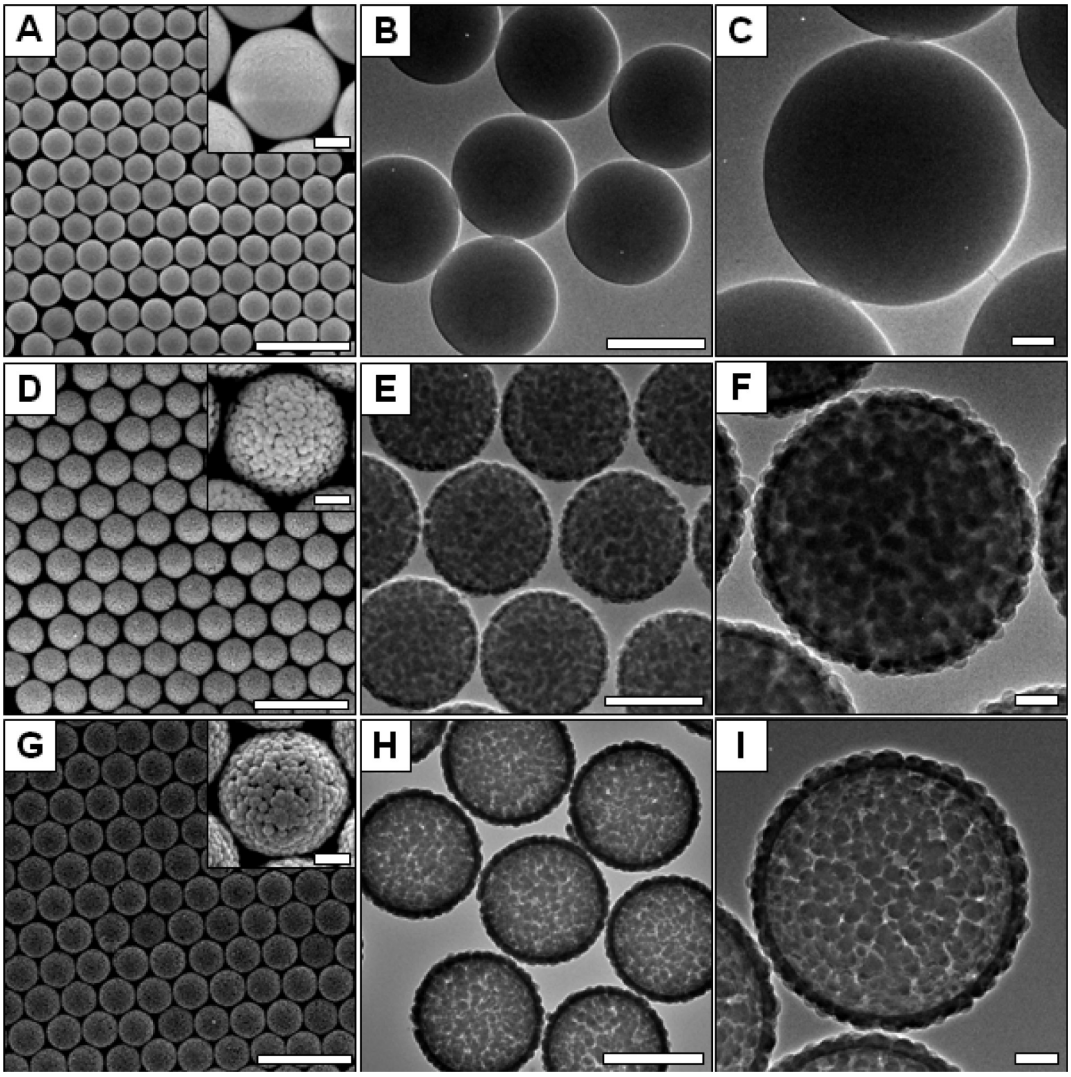

Figure 1. (A, D, G) SEM and (B, C, E, F, H, I) TEM images of the as-synthesized (A−C) PS beads, (D−F) PS@SiO_2 core/shell composite beads, and (G−I) MSHMs. Scale bars: (A, D, G) 2 μm; (B, E, H) 500 nm; (C, F, I) 100 nm; (insets in A, D, G) 200 nm.

the Supporting Information). It is believed that the small increase in size was due to the slight relaxation in silica shell after PS core removal. More remarkably, through holes with irregular shapes could be easily observed in the silica shells under SEM observations (inset in Figure 1G), suggesting the successful formation of the macrophorous silica hollow microspheres, namely MSHMs. It should be noted the dimension of holes observed under SEM was less than the real value because of a layer of gold sputtered prior observations. TEM images revealed typical hollow structures with the shell thickness of around 40 nm, the same as the dimension of primary silica nanoparticles in PS@SiO_2 composite spheres before core removal (Figure 1H). The characteristic through holes with typical diameters larger than 50 nm in the shells could be clearly observed (Figure 1I) (see large-magnification TEM and SEM images in see Figure S4 in the Supporting Information), further confirming the formation of MSHMs. Due to the presence of large through-holes at the shell, the core removal process in toluene was fast, usually less than 30 min. Only two weight-loss stages in TGA measurement were observed for the as-obtained MSHMs (see Figure S3 in the Supporting Information), i.e., below 300 and above 400 °C, which corresponded to the evaporation of physically adsorbed water and residual solvent, and the decomposition of silica-bonded groups such as −OH and/or unhydrolyzed −OR, respectively.[14] This confirmed the complete removal of PS core during the dissolution process, because the decomposition of polystyrene mainly occurred in the temperature range from 300 to 400 °C. Alternatively, MSHMs could be also obtained by calcining PS@SiO_2 composite beads at 450 °C for 1 h, as shown in see Figure S5 in the Supporting Information. Again, because of the presence of large through-holes, collapsed MSHMs were seldom observed after calcination because the holes could act as channels for effective transfer of decomposed molecules. Moreover, the specific surface area of MSHMs estimated through nitrogen sorption isotherms was 49.0 m^2/g. By taking 2.2 g/cm^3 as the density of silica, the diameter for primary silica nanoparticles was estimated to be 56.6 nm, slightly larger than the SEM and TEM observations. This is easy to understand, as we assumed that the silica nanoparticles were isolated and untouched from each

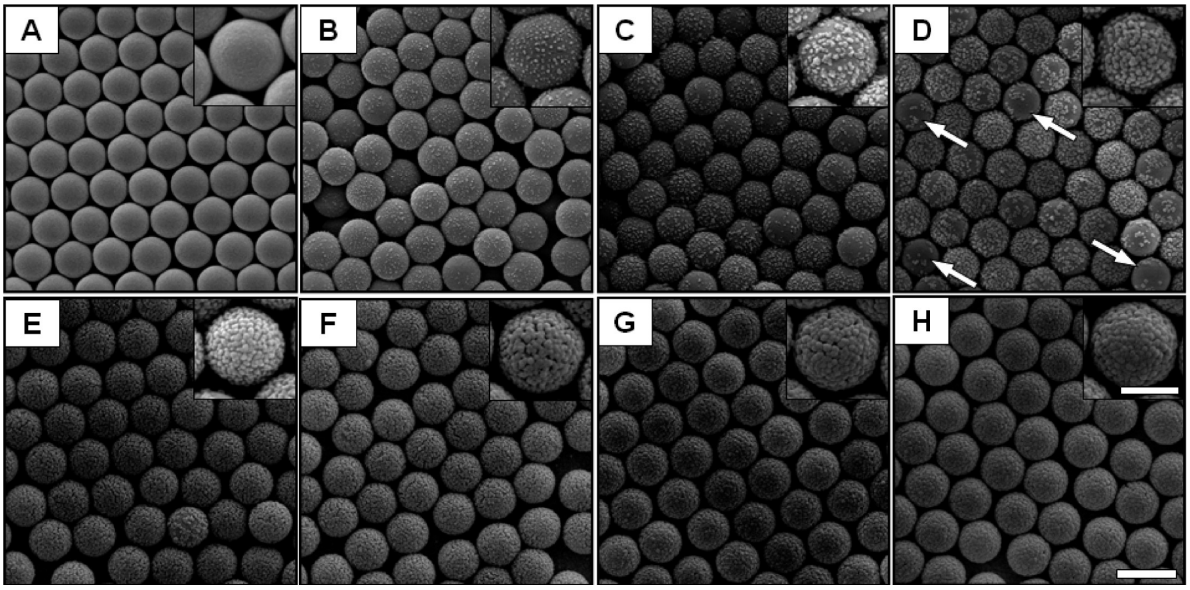

Figure 2. SEM images of PS@SiO_2 core/shell composite beads obtained at different reaction times: (A) 1, (B) 3, (C) 6, (D) 10, (E) 15, (F) 25, (G) 40, and (H) 60 min. The white arrows in D show the PS beads with poor coverage of silica nanoparticles. All the images and corresponding insets are in the same magnification, and scale bars are 1 μm and 500 nm, respectively.

other in calculation, whereas the particles were connected with adjacent ones in MSHMs.

To obtain MSHMs with well-defined shell morphology, it is essential to first fabricate the corresponding PS@SiO_2 core/shell microspheres. Figure 2 presents the morphology evolution of the composite beads obtained upon various silica deposition times, i.e., 1, 3, 6, 10, 15, 25, 40, and 60 min. As shown in Figure 2A, no silica deposition on the PS surface was observed when the reaction was only allowed for 1 min. TEM observations also revealed that the PS surfaces were completely smooth after 1 min deposition (see Figure S6A−B in the Supporting Information). However, after 3 min, nanosized silica seeds (size ~10 nm) were evenly distributed on the surface, corresponding to the white spots under SEM observations (Figure 2B). At this stage, the silica seeds were isolated from each other and had irregular shapes (see Figure S6C−D in the Supporting Information). The average distance among the silica seeds was estimated to be 80−100 nm. The silica seeds quickly grew bigger in dimension to around 25 nm after another 3 min (Figure 2C), which remained untouched from each other (see Figure S6E−F in the Supporting Information). When the reaction was allowed for 10 min, the dimension of silica particles continued to increase, and coalesce among adjacent nanoparticles was clearly observed (Figure 2D). However, complete silica shells at this stage were not formed yet. This was evident by the appearance of some composite microspheres with poor coverage of silica nanoparticles, indicated by the white arrows (Figure 2D). The coalescence among silica nanoparticles continued to increase after another 5 min reaction (Figure 2E). As shown in Figure 2F, after 25 min of reaction, further increase in dimension (size ~ 40 nm) of the silica nanoparticles led to a complete connection among them, thus forming a complete macroporous shells. This fully connected shell greatly reduced the possibility of silica fall-offs, as poorly covered PS beads were seldom observed. As the reaction proceeded to 40 min, further increase in the silica dimension led to a higher degree of silica coverage (Figure 2G). Finally, complete coverage with silica shells was observed after 1 h, and virtually no holes left at the PS surface (Figure 2H). TGA results also indicated that the silica content for PS@SiO_2 composite beads gradually increased with increase in reaction time (see Figure S7 in the Supporting Information).

The PS@SiO_2 composite beads prepared at various silica deposition times were further treated in toluene to remove the cores, in order to study the effects of deposition time on formation of the silica hollow structures. As shown in Figure 3A, no intact hollow spheres were observed but macroporous silica sheets when the deposition time was 10 min. The silica sheets consisted of primary silica nanoparticles with size of around 30 nm. Moreover, it was possible to differentiate the interior surface, which was previously attached to the PS beads, with exterior ones. The top surface for the silica sheet indicated by the white arrow was attached to the PS surface before core removal, as it was much smoother compared with that indicated by the black arrow (inset in Figure 3A. The enlarged image is shown insee Figure S8A in the Supporting Information). At this stage, the macrosized holes could be clearly observed in the incomplete shells, forming networklike structures, as shown in a typical TEM image (see Figure S8B in the Supporting Information). For 15 min composite beads, hollow spheres could be obtained after dissolution, although there were substantial amount of incomplete ones (Figure 3B). This was due to the low degree of coalescence among silica nanoparticles in the shells, which also resulted in hollow spheres with deformed shapes (see

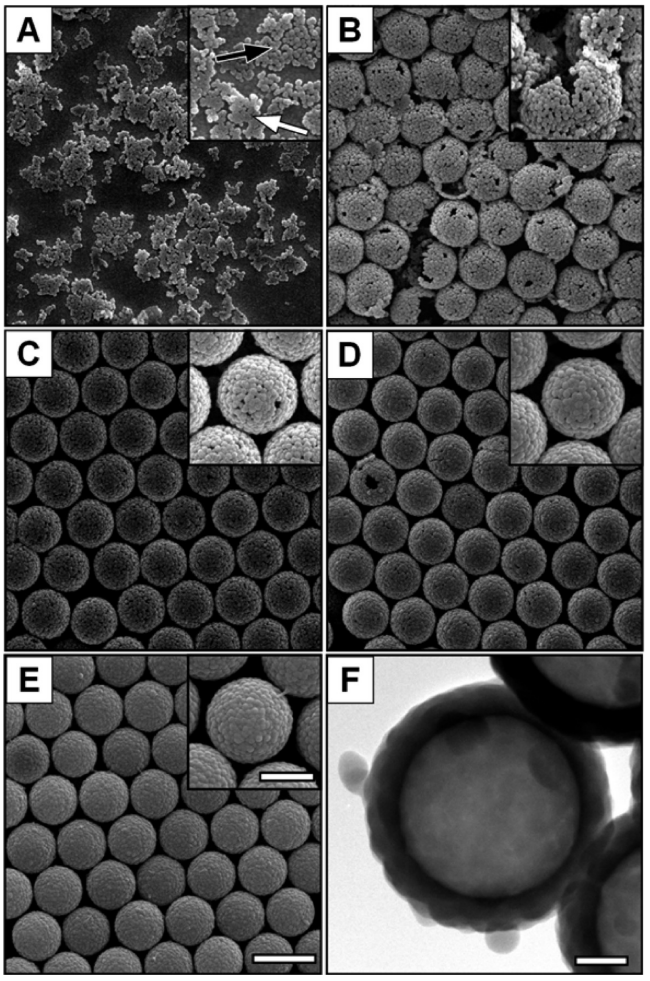

Figure 3. SEM images of products obtained by dissolving the PS cores using corresponding PS@SiO_2 core/shell beads obtained at (A) 10, (B) 15, (C) 25, (D) 40, and (E) 60 min. (F) TEM images of the products after hole close-up through further silica coating. Image A−E and corresponding insets are in the same magnifications, respectively. Scale bars: (A−E) 1 μm, (insets) 500 nm, and (F) 200 nm.

Figure S9 in the Supporting Information). When 25 min PS@SiO_2 particles were used, monodisperse MSHMs without collapse were obtained (Figure 3C). Low-magnification SEM image shows that the obtained MSHMs readily formed hexagonal close-packed 2D structures after solvent evaporation at room temperature (see Figure S19 in the Supporting Information). 40 min PS@SiO_2 particles could be also used to obtain hollow spheres; however, both the number and the size of the through-holes reduced dramatically as the result of silica growth (Figure 4D). Nearly no through-holes were observed when 60 min PS@SiO_2 particles were used (Figure 4E). Moreover, it was found that the dissolution process became increasingly slower for PS@SiO_2 particles obtained at longer reaction times. Core removal could be completed within 30 min for 25 min composite particles. However, TGA results indicated that almost no PS dissolution occurred after dissolving 60 min sample even for 24 h (see Figure S11 in the Supporting Information). TEM & SEM observations also confirmed the presence of PS cores after the treatment by toluene (see Figure S12 in the Supporting Information). This reduction in dissolution speed was resulted from the absence of macro-sized through holes in the shells, which could greatly facilitate the dissolution process. Moreover, the through holes in the shells of MSHMs could be easily closed up by a further silica coating, thus forming dense hollow spheres, as shown in Figure 3F. SEM images also showed the shells were fully covered without holes after this treatment (see Figure S13 in the Supporting Information).

In this process, the formation of isolated primary silica nanoparticles at the PS surface is the key to forming the macroporous shell. As shown in Scheme 1, silica seeds are first formed after introduction of ammonia hydroxide, and immediately attached onto the PVP-modified PS surface within 3 min (Scheme 1B). It is known that PVP is usually used as surface linker to assist attachment of various materials onto another substrate. For example, Graf et al. successfully obtained nanoparticle-decorated silica spheres by using PVP as a surface coupling agent.[43] Zou et al. fabricated dense silica hollow spheres with PVP-modified PS beads.[44] Subsequent growth of silica nanoparticles leads to necking and coalescence among adjacent nanoparticles, hence forming an intact silica shell (Scheme 1C). The well-defined MSHMs are obtained by removing the PS core through dissolution in toluene or calcination at 450 °C, which have characteristic macroporous shells resulted from incomplete coverage of silica nanoparticles (Scheme 1D). Post close-up of through holes in the shells were easily achieved through further silica coating process. Interesting close-packed patterns formed by the obtained MSHMs could be clearly observed under TEM because of their good monodispersity and macroporous shells (see Figure S14 in the Supporting Information).

We next demonstrate the usage of the as-prepared MSHMs as novel microcollectors to capture nanoparticles from external solutions. We first chose hydrophilic Au nanoparticles (diameter ~14 nm) as modal particles, which were prepared separately through the classic sodium citrate reduction method (see Figure S1 in the Supporting Information). It was found that MSHMs could efficiently capture Au nanoparticles by utilizing the through-holes in the shells as channels, where Au nanoparticles migrated from external environment to the interior space of MSHMs. As shown in an SEM image (Figure 4A), Au nanoparticles, corresponding to the white spots, were clearly observed inside a crushed MSHM, while few Au particles were observed at the outer surface of MSHMs. TEM also revealed successful loading of Au nanoparticles within the hollow interiors (Figure 4B−C). As the TEM sample was dried during preparation, Au nanoparticles were resided at the inner surface of MSHMs. Crushed MSHMs gave us a better visualization of this complex structure, as shown in Figure 4D. It was easy to notice that the majority of nanoparticles attached on the inner shell (black arrow),

(43) Graf, C.; Vossen, D. L. J.; Imhof, A.; van Blaaderen, A. *Langmuir* **2003**, *19*, 6693–6700.
(44) Zou, H.; Wu, S.; Ran, Q.; Shen, J. *J. Phys. Chem. C.* **2008**, *112*, 11623–11629.

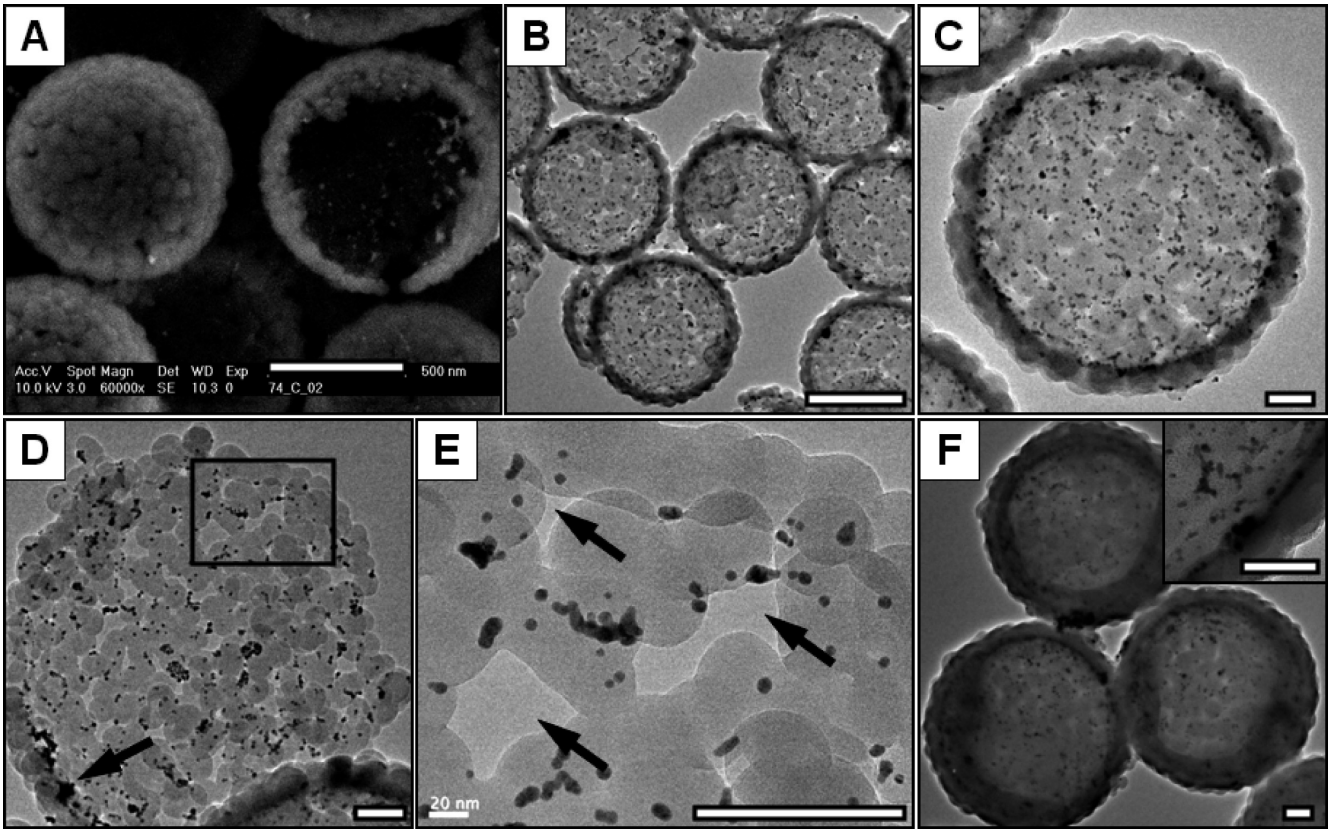

Figure 4. (A) SEM and (B, C) TEM images of the Au-loaded MSHMs. (D) TEM image of a crushed MSHM, illustrating a single macroporous shell with Au nanoparticles resided at the inner surface. (E) TEM image for an enlarged view of the rectangle portion in D. Black arrows indicate the through holes. (F) TEM image of the product after hole close-up for Au-loaded MSHMs. (Inset of F) Complete coverage of the silica shell. Scale bars: (A, B) 500 nm, (C−F and inset of F) 100 nm.

Scheme 1. Schematic Representation of the Preparation of MSHMs through a Template-Assisted Method: (A) PVP-Modified PS Beads; (B) SiO_2-Seeded PS Beads; (C) PS@SiO_2 Composite Beads; and (D) MSHMs

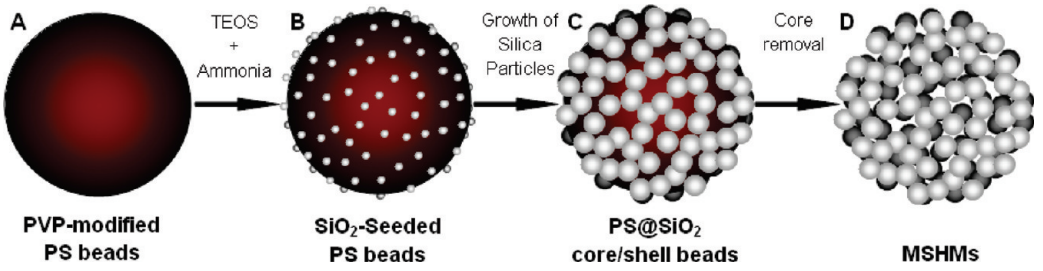

and very few were observed on the outer surface. An enlarged area indicated by a rectangle is shown in Figure 4E, where the macrosized holes (indicated by the arrows) together with the loaded Au nanoparticles could be clearly seen. The through holes in Au-loaded MSHMs could be also facilely closed up through further silica coating, as shown in Figure 4F. This type of internal-decorated hollow microspheres has been synthesized previously through either attachment of particles at core surface or secondary reaction through the shells.[45−48]

Compared with the previous synthetic approaches, our method offers the following several advantages: (1) large amount of nanoparticles can be loaded; (2) nanoparticles with desired structures and properties can be engineered separately before loading; (3) more than one type of nanoparticles can be loaded simultaneously.

Moreover, we conducted a quantitative study on the loading efficiency of Au nanoparticles. Increasing amounts of MSHMs, i.e., 0.8, 1.6, 2.4, and 3.2 mg, were dispersed in 2 mL of Au aqueous solutions, respectively. MSHMs after loading were separated through low-speed centrifugation. The supernatant solutions after centrifugation were denoted as SPT01, 02, 03, 04, respectively, while the Au-loaded MSHMs were denoted as PPT01, 02, 03, 04, respectively. Figure 5A demonstrates the UV−vis absorption spectra for original Au colloid and

(45) Kim, M.; Sohn, K.; Bin, N. H.; Hyeon, T. *Nano Lett*. **2002**, *2*, 1383–1387.
(46) Kamata, K.; Lu, Y.; Xia, Y. *J. Am. Chem. Soc*. **2003**, *125*, 2384–2385.
(47) Kim, J. Y.; Yoon, S. B.; Yu, J. S. *Chem. Commun*. **2003**, 790–791.
(48) Cheng, D. M.; Zhou, X. D.; Xia, H. B.; Chan, H. S. O. *Chem. Mater*. **2005**, *17*, 3578–3581.

SPT01−04. It could be easily observed that the intensity at extinction peak of Au colloid ($\lambda_{max} = 526$ nm) gradually reduced with increasing amount of MSHMs used, also shown in Table 1. This indicated that more nanoparticles were captured by increasing the amount of MSHMs used, i.e., from 62.96%, to 83.33%, to 87.78%, to 91.48%. This result also agreed with the results of ICP analysis (Table 1). Particularly for SPT04, almost zero absorption at wavelength of 526 nm was observed in the corresponding UV−vis spectrum and its Au concentration was beyond the ICP detection limit. The inset photograph in Figure 5A shows the SPT01−04 solutions together with the original Au colloid, from which we could clearly see that the red color resulted from the surface plasmonic resonance of Au nanoparticles was gradually reduced, indicating that concentrations of Au nanoparticles were gradually decreased with increase in the amount of MSHMs used. Figure 5B shows the UV−vis spectra for Au-loaded MSHMs (i.e., PPT01−04). First, λ_{max} did not have any significant shift, suggesting that the surface chemistry of Au nanoparticles was not affected even when they were captured inside the hollow structure. Second, it was noticed that the background absorption increased

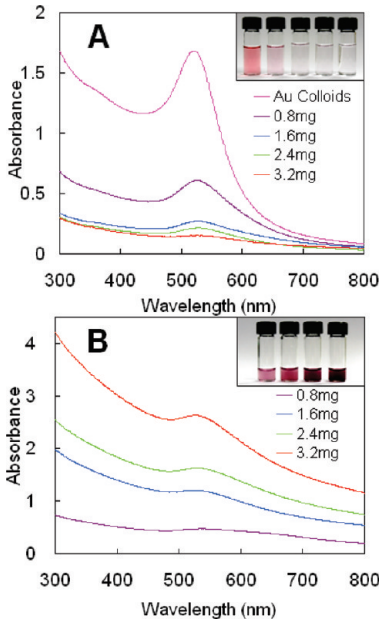

Figure 5. (A) UV−vis absorption spectra of the original Au aqueous colloid, and supernatant solutions with Au-loaded MSHMs removed through centrifugation, i.e., SPT-01, 02, 03, and 04. (B) UV−vis absorption spectra of Au-loaded MSHMs, i.e., PPT-01, 02, 03, and 04.

from PPT01 to 04 linearly, which was due to the linear increase in MSHMs used. Lastly, the increase in the relative intensity of λ_{max} from PPT01 to 04 indicated that more Au nanoparticles were captured by MSHMs and subsequently separated through centrifugation. The inset photograph in Figure 5B shows samples PPT01−04, where the color became darker from 01 to 04, confirming more Au nanoparticles were captured. Moreover, the number of nanoparticles within each MSHM could be roughly estimated by taking some simple assumptions, as shown in the last column of Table 1. It was found that the calculated results were comparable with TEM observations.

Lastly, we found that the as-synthesized MSHMs could be also directly used for capturing hydrophobic nanoparticles from nonpolar solutions. As shown in Figure 6A, hydrophobic SPIONs prepared through a high-temperature decomposition route could be readily loaded within MSHMs. selected area electron diffraction (SAED) pattern acquired at the crushed pieces of SPION-loaded MSHMs matched well with the magnetite phase of SPIONs, and the big white area in the center was resulted from the amorphous silica shell. Uniformly distributed SPIONs and holes could be clearly observed in the shells (see Figure S16 in the Supporting Information). Energy-dispersive X-ray (EDX) analysis also confirmed the presence of SPIONs within the hollow interiors (see Figure S17 in the Supporting Information). The as-prepared SPION-loaded MSHMs dispersed in ethanol could be easily separated by a magnet, demonstrating a strong magnetic response (Figure 6C−D). Moreover, more than one type of nanoparticles could be loaded with MSHMs simultaneously. As a demonstration, hydrophobic SPIONs and CdSe/ZnS quantum dots (QDs) were both encapsulated inside MSHMs (Figure 6B), which was verified by EDX analysis (see Figure S17 in the Supporting Information). Most of the particles were successfully captured in the interior space of MSHMs, although some nanoparticles adhered at the external surface (inset of Figure 6B). These as-prepared QD/SPION-loaded MSHMs emitted red fluorescence under UV illumination (365 nm), which could be also separated by a magnet (Figure 6E−F). A very small red shift of the photoluminescence spectra was observed after loading (636.5 to 640.5 nm), and the half-maximum range did not have any significant change (Figure 6G). This type of composite microspheres can be potentially used as multifunctional

Table 1. Loading of Au Nanoparticle with Different Amounts of MSHMs and Estimation of Nanoparticle Loading Efficiency by Using Both ICP and UV−Vis Results[a]

				removal efficiency (%)		Au nanoparticles per MSHM	
sample	MSHMs (mg)	conc. (ppm)	λ_{max} intensity	ICP[c]	λ_{max}[d]	ICP[c]	λ_{max}[d]
SPT01	0.8	28.63	0.625	63.77	62.96	682	673
SPT02	1.6	9.63	0.281	87.81	83.33	469	445
SPT03	2.4	4.06	0.206	94.86	87.78	338	313
SPT04	3.2	ND[b]	0.143		91.48		244

[a] 2.2 and 19.3 g/cm^3 were used as the densities of MSHMs and Au nanoparticles. A perfect hollow sphere modal with inner and outer diameters of 705 and 784 nm was assumed. Original Au colloid concentration determined from ICP analysis was 79.01 ppm, and intensity at λ_{max} (526 nm) was 1.688. [b] Not detected. [c] Values were calculated from ICP results [d] Values were calculated from λ_{max} intensity in UV−vis spectra.

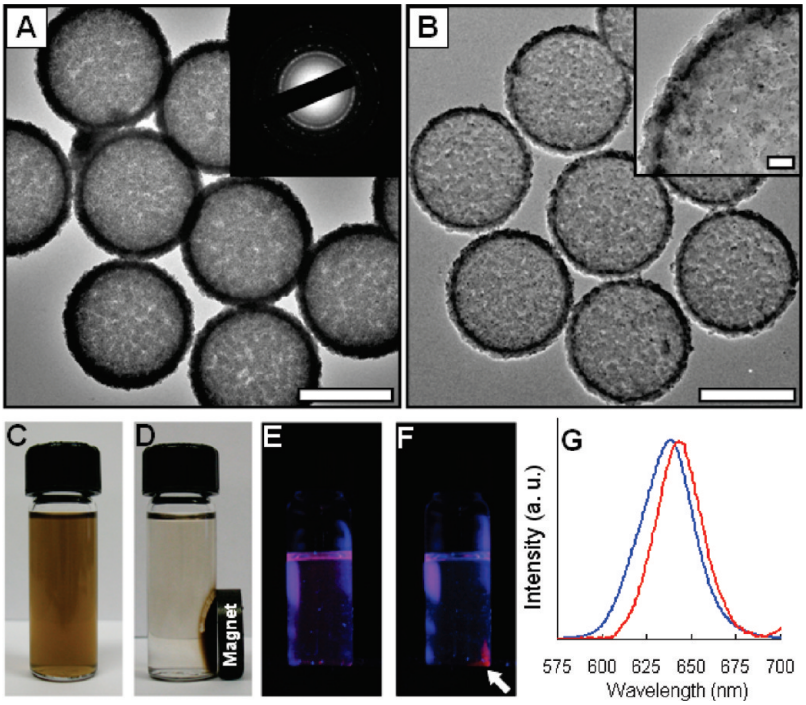

Figure 6. TEM images of (A) SPION-loaded MSHMs and (B and inset) QD/SPION-loaded MSHMs. Photographs of (C) SPION-loaded MSHMs dispersed in ethanol, (D) sample in C after magnetic separation, (E) QD/SPION-loaded MSHMs dispersed in ethanol under UV illumination (365 nm), and (F) sample in E after magnetic separation showing concentrated red fluoresce emitted from the multifunctional particles (white arrow). (G) Photoluminescence (PL) spectra for original QDs (blue) and QD/SPION-loaded MSHMs (red). Scale bars: (A, B) 500 nm, (inset of B) 50 nm.

nanoplatform for various biological applications after careful surface modification and functionalization, for example, simultaneous guided drug delivery, tracking, and monitoring.[39,49] It is believed that other functional microspheres can be readily obtained by loading various kinds of nanoparticles, like noble metal nanoparticles, which may have potential applications in catalysis.

Conclusions

In conclusion, we demonstrated a facile route to prepare monodisperse MSHMs with large through holes (size > 50 nm) in their shells. The formation of PS@SiO_2 composite microspheres is essential to prepare MSHMs with tailored structure. The continuous macroporous silica shells on PS templates were formed when the silica deposition time was optimized at 25 min, leading to the successful fabrication of MSHMs with well-defined microstructure. The as-synthesized MSHMs could be used as efficient microcollectors to capture and load either hydrophilic or hydrophobic nanoparticles from polar or nonpolar solvents. Quantitative analysis indicated more nanoparticles could be captured by increasing the amount of MSHMs used. The through holes of MSHMs could also be readily closed up through a post silica coating process, so as to permanently encapsulate entities inside the hollow spheres. Composite MSHMs loaded with various functional nanoparticles may find significant applications in various fields, including biomedicine, catalysis, etc.

Acknowledgment. This work is supported by the Singapore MOE's ARF Tier 1 funding WBS R-284-000-050-133.

Supporting Information Available: Size distributions, TGA analysis, and additional SEM and TEM images (PDF). This material is available free of charge via the Internet at http://pubs.acs.org.

(49) Liong, M.; Lu, J.; Kovochich, M.; Xia, T.; Ruehm, S. G.; Nel, A. E.; Tamanoi, F.; Zink, J. I. *ACS Nano* **2008**, *2*, 889–896.